DOI: 10.1002/chem.200801638

Magnetic Interactions and Magnetic Anisotropy in Exchange Coupled 4f–3d Systems: A Case Study of a Heterodinuclear Ce^{3+}–Fe^{3+} Cyanide-Bridged Complex

Lorenzo Sorace,*[a] Claudio Sangregorio,[a] Albert Figuerola,[b] Cristiano Benelli,[a] and Dante Gatteschi[a]

Dedicated to the memory of Alessandro Bencini (1951–2008)

Abstract: We report here a detailed single-crystal EPR and magnetic study of a homologous series of complexes of the type Ln–M (Ln = La^{III}, Ce^{III}; M = Fe^{III}, Co^{III}). We were able to obtain a detailed picture of the low-lying levels of Ce^{III} and Fe^{III} centres through the combined use of single-crystal EPR and magnetic susceptibility data. We show that classical ligand field theory can be of great help in rationalising the energies of the low-lying levels of both the transition-metal and rare-earth ions. The combined analysis of single-crystal EPR and magnetic data of the coupled system Ce–Fe confirmed the great complexity of the interactions involving rare-earth elements. With little uncertainty, it turned out clearly that the description of the interaction involving the lowest lying spin levels requires the introduction of the isotropic, anisotropic and antisymmetric terms.

Keywords: antisymmetric exchange · cerium · EPR spectroscopy · exchange interactions · iron · lanthanides · magnetic properties

Introduction

Designing molecular systems with expected properties is certainly one of the main challenges of chemistry in the twenty-first century. Success in this field would allow the development of new types of materials and devices and provide a significant breakthrough based on a complete understanding of the relationship between molecular structures and properties.

A field in which the design process is perhaps most difficult is molecular magnetism.[1] Many important steps forward have been made in the last few years by developing new classes of low dimensional magnetic materials,[2] such as room-temperature molecular ferrimagnets;[3] new classes of nanomagnets,[4] including single-molecule magnets (SMM)[5] and single-chain magnets (SCM);[6] and chiral[7] and switching magnets[8] to mention just a few. The ideal process in designing new molecular magnets requires choosing the best suited building blocks that must be connected in order to display suitable magnetic interactions. However, this is only the first step, because it is also necessary to have control of the magnetic anisotropy, which critically determines the behaviour of the magnets, like, for instance, the SMM and SCM behaviours that require an easy axis (Ising) type magnetic anisotropy.[9]

Several different sources of magnetic anisotropy are used, but all of them share the need of introducing some orbital component in the investigated systems. In the condensed phase, the orbital component is often quenched by crystal field and Jahn–Teller effects, but spin–orbit coupling reintroduces it to some extent.[10] An efficient way of introducing magnetic anisotropy is by using rare-earth ions, which, with their internal 4f valence orbitals, conserve large orbital contributions. However, while this is an advantage in terms of magnetic anisotropy, it represents a major drawback in terms of efficient coupling between the molecular building

[a] Dr. L. Sorace, Dr. C. Sangregorio, Prof. C. Benelli, Prof. D. Gatteschi
UdR INSTM and Dipartimento di Chimica
Università di Firenze, Via della Lastruccia 3
50019 Sesto Fiorentino (FI) (Italy)
Fax: (+39) 055-457-3372
E-mail: lorenzo.sorace@unifi.it

[b] Dr. A. Figuerola
Departament de Química Inorgànica i
Institut de Nanociència i Nanotecnologia
Universitat de Barcelona, Av. Diagonal 647
08028 Barcelona (Spain)

Supporting information for this article is available on the WWW under http://dx.doi.org/10.1002/chem.200801638.

blocks. If the coupling between d orbitals is typically of the order of 100 K, then the coupling between f orbitals is around 1 K.[11]

To maximise the inter-ion coupling while maintaining a sizeable magnetic anisotropy, systems in which 4f ions are coupled to transition-metal ions or organic radicals are often used. In this way it has been possible to obtain systems that order as ferrimagnets at about 5 K.[12] In the field of molecular nanomagnets, magnetic clusters with large anisotropy and SMM behaviour[13] as well as systems with SCM behaviour were obtained.[14,15] Notwithstanding these successes, the actual understanding of the magnetostructural correlations affecting exchange coupling interactions and magnetic anisotropy in molecular systems containing rare-earth ions is often obscured by the low symmetry of the lanthanide coordination sphere and by the presence of unquenched orbital components. This makes the use of simple spin Hamiltonian approaches and related ligand field theories, which are so useful in the interpretation of the magnetic properties of 3d molecular magnets, problematic.[16] As a consequence, the understanding of these phenomena has remained, up to now, at a mainly qualitative level, with most of the information having been gained by the diamagnetic substitution method.[17] In this approach, the paramagnetic species coupled to a rare-earth element (RE) is substituted by a diamagnetic one, while preserving the molecular structure. This allows the comparison of the χT value of the magnetic pair, REp–TMp, with those of the REd–TMp and REp–TMd couples (RE = rare earth, TM = transition metal, p = paramagnetic and d = diamagnetic). If the sum of the magnetisation values of the pairs containing a diamagnetic centre equals that of the magnetic one, then it can be safely assumed that no interaction is operative, while significant deviations point out ferro- or antiferromagnetic interactions.

While this might be a powerful approach, it has been used, up to now, only for powder measurements,[18] thus failing to provide any detailed information about the anisotropic features of the species involved. In fact, due to the unquenched orbital contributions, the spin Hamiltonian needed for the interpretation of the magnetic properties of 3d–4f pairs is much more complex than for 3d pairs. Some attempts in this direction have been made recently by Tangoulis et al., who fitted the data obtained by a combination of techniques with only one set of anisotropic parameters.[19,20] However, in order to avoid overparametrisation in the fitting procedures, some restrictions had to be considered: an axial symmetry of the exchange was assumed for the analysis of the magnetic data, as well as the collinearity of the **g** tensors of Ln and M.

The deviations occurring due to these restrictions should not be underestimated and make the need for single-crystal magnetic analysis of simple isostructural compounds evident, to obtain this information and to test the validity of the approach on a quantitative level. A further point to be considered is the relative importance of the different contributions to the global anisotropy of the system and in particular of the antisymmetric (AS) exchange contribution.[21] This is in fact a rather elusive term that is often invoked, but rarely unequivocally demonstrated. It is, however, certain that it must play a role in lanthanide magnetism, and molecular compounds may be ideal for the investigation of AS exchange.

Recently, some of us[22] reported a series of heterodinuclear $[Ln(dmf)_4(H_2O)_3(\mu\text{-}CN)M(CN)_5]\cdot n H_2O$ complexes (Ln–M, in which Ln is a lanthanide ion, $M = Fe^{3+}$, Co^{3+}, DMF = *N*,*N*′-dimethylformamide), which provided the unique opportunity to have an isostructural series in which paramagnetic ions, like cerium(III) and low-spin iron(III) can be substituted by diamagnetic ions like lanthanum(III) and low-spin cobalt(III).[22] Polycrystalline powder magnetic and EPR measurements provided some preliminary information.[19] Improvements in the synthesis of the three compounds of interest in the present study made the preparation of high-quality single-crystal samples possible and allowed us to perform an exhaustive single-crystal analysis by both EPR and magnetic measurements.

The wealth of information derived undoubtedly provides scientists with a clearer and more detailed picture of the magnetic anisotropy and electronic structure of paramagnetic systems with non-quenched orbital momenta. We propose this as a case study that may bring an important contribution to the understanding of the magnetic properties of molecular magnets involving rare earth ions, while, at the same time, showing the limitations of predicting the magnetic coupling and the magnetic anisotropy in these systems.

Single-crystal EPR measurements were used as a first and most reliable source of data due to its peculiar sensitivity to the local symmetry of the molecule.[23,24] Anisotropic data coming from single paramagnetic ions can indeed be obtained if the coupling between the two centres is negligible. In contrast, data supplied by magnetic measurements, even when single-crystal samples are used, are related to the symmetry of the crystal and hence information concerning the single ion is lost if more than one inequivalent magnetic centre is present in the crystal.[25] For this reason the key step of the approach consisted in the determination of the magnitudes and orientations of the three components of the **g** tensors for the iron(III) and cerium(III) ions, when using non-coupled systems (La–Fe and Ce–Co). Also, a preliminary study of the anisotropy in the exchanged Ce–Fe system is presented and derived from this technique. After that, a description of the single-crystal magnetic data for the Ce–Co and Ce–Fe compounds is provided, which was then also used as valuable data to confirm previous results.

In the Discussion section, and using all of the above-derived data from EPR measurements, a good description of the electronic structure of both isolated paramagnetic ions in La–Fe and Ce–Co compounds is given (energy spectra, orbital composition of the ground states and ligand field parameters). Concerning the exchanged-coupled Ce–Fe system, a detailed analysis of the interaction term between the two ions was conducted in order to elucidate the weight of the different possible contributions (isotropic, anisotropic and antisymmetric). All conclusions extracted from EPR

measurements were further confirmed by single-crystal magnetic measurements in the case of Ce–Co and Ce–Fe compounds.

Results

Structure: The molecular structure of the Ln–M complexes has been reported previously.[22] We will quickly review its basic features in order to provide the reader with a basis to follow the discussion on the magneto–structural correlation. The three complexes are isostructural with a monoclinic unit cell containing four discrete heterodinuclear molecules and crystallising in the space group $P2_1/n$. The basic structural unit (see Figure 1) consists of the association through one

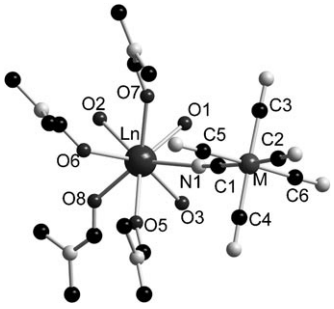

Figure 1. Diamond view of the basic structural unit of $[Ln(DMF)_4(H_2O)_3M(CN)_6]$ ($Ln = La^{III}$, Ce^{III}; $M = Co^{III}$, Fe^{III}).

cyanide bridge of fragments of $\{M(CN)_6\}$ (with $M = Fe^{3+}$ or Co^{3+}) and $\{Ln(dmf)_4(H_2O)_3\}$ (with $Ln = La^{3+}$ or Ce^{3+}); derivatives with Pr^{3+}, Sm^{3+}, Tm^{3+}, and Yb^{3+} have also been reported. A water molecule crystallises for each molecular unit.[22]

The Ln^{3+} ion has a coordination number of eight, with seven oxygen atoms and the nitrogen atom of the cyanide bridge. Even though in reference [22] it was stated that the coordination polyhedron around the central ion could be considered a distorted dodecahedron, polytopal analysis[26] indicates values which are very close to the ideal for a bicapped trigonal prism (see Table 1), as also evidenced in Figure 2.

On the other hand the coordination sphere of the M^{3+} ions consists of the six cyanide carbon atoms, which produce a distorted octahedron. Its structural parameters are in agreement with data reported in the literature for other M^{3+}–cyanide derivatives.[27] It should be noted that no remarkable difference among the M–C distances for bridged and non-bridging cyanides exists. The torsion angle among the two units, M-CN-Ln, is 39.7°, indicating a substantial deviation from co-planarity.

Another important parameter for the analysis of the magnetic data is the M–Ln distance: Ce–Co 5.539(3) Å, La–Fe 5.622(2) Å and Ce–Fe 5.581(4) Å. Finally, it should be pointed out that the neutral dinuclear units are linked by

Table 1. Experimental dihedral angles for $[Ce(DMF)_4(H_2O)_3Co(CN)_6]$ and ideal values for SAPR-8 (square antiprism) and BCTP-8 (bicapped trigonal prismatic) geometries.[a]

	Experimental	BCTP-8	SAPR-8
O5(N1O8)O7	24.11	21.8	0.0
O1(O2O3)O8	2.90	0.0	0.0
O5(O2O8)O6	47.68	48.2	52.4
O1(N1O3)O7	46.12	48.2	52.4
O5-O1-O7-O6	17.68	14.1	24.5
O8-O3-O2-N1	16.56	14.1	24.5

[a] A(BC)D is the dihedral angle between the ABC plane and the BCD one. A-B-C-D is the dihedral angle between the (AB)CD plane and AB(CD) in which (AB) indicates the midpoint of the AB edge.

hydrogen bonds in a 3D network. The 3D network is made of alternating Ln–M dinuclear entities linked by hydrogen bonds between the five terminal CN groups of the $\{M(CN)_6\}$ fragment, the three oxygen atoms of the H_2O ligand of the $\{Ln(dmf)_4(H_2O)_3\}$ fragment and the water molecules from crystallisation.

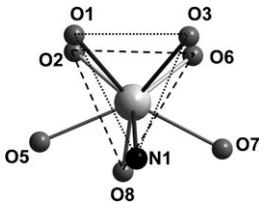

Figure 2. Detailed view of the coordination sphere of the Ln centre in $[Ln(DMF)_4(H_2O)_3M(CN)_6]$ showing the bicapped trigonal prismatic geometry.

EPR spectra: An analysis of the polycrystalline powder X-band EPR spectra of La–Fe, Ce–Co and Ce–Fe recorded at 4 K has recently been reported.[19] Here, we will review the main results. The spectrum of La–Fe is typical for a $^2T_{2g}$ ion in a low-symmetry environment with three signals occurring, on the basis of simulated spectra, at $g_1 = 2.47$, $g_2 = 2.04$ and $g_3 = 0.72$. These values are similar to those reported for potassium ferricyanide doped in an analogous cobalt compound.[28]

The spectrum of Ce–Co corresponds to an effective spin $S = {}^1/_2$, originating from the crystal field splitting of the ground $^2F_{5/2}$. The simulation of the spectra yielded $g_1 = 1.77$, $g_2 = 0.98$, $g_3 = 2.82$, which are compatible with the values reported as the results of an investigation on cerium(III) doped in yttrium aluminium garnets.[29]

The spectrum of Ce–Fe is different from the sum of the individual spectra of La–Fe and Ce–Co, indicating that the two paramagnetic ions are interacting with each other. A simple interpretation of this spectrum is not possible, as the magnetic studies showed that the exchange coupling between cerium and iron is weak.[22]

The angular dependence of single-crystal X-band EPR spectra of La–Fe in three orthogonal planes is shown in Figure 3 (top). The reference frame is as follows: X is along the [101] direction, Y is in the b direction [010] and Z is perpendicular to both X and Y. For general orientation of the magnetic field, the spectra show two signals due to the two magnetically non-equivalent units present in the monoclinic unit cell. As expected, for a field oriented in the XZ plane and parallel to Y, only one signal is observed.

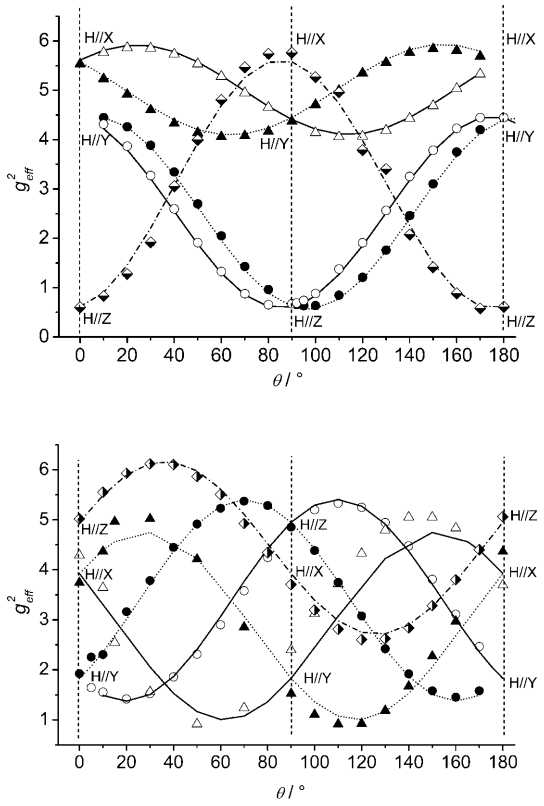

Figure 3. Angular dependence of the EPR resonance fields for single crystals of La–Fe (top) and Ce–Co (bottom) rotating in three orthogonal planes and best fit curves. Circles indicate rotations around X, diamonds around Y and triangles around Z; the full and empty show the signals from the two magnetically inequivalent individuals in the first and third rotations.

The standard analysis[30] of the three orthogonal rotations, based on an effective $S=^1/_2$ spin, provided the $\mathbf{g}^2$ tensors, and from this the corresponding **g** matrices and principal g values which are reported in Table 2 were obtained. Due to the monoclinic nature of the crystal, four different possible combinations of angular dependences, corresponding to different orientations of the **g** tensor with respect to the molecular frame, have to be considered (the complete set of tensors is reported in Table S1 in the Supporting Information). All of them were fitted giving principal g values in agreement with those obtained by analysis of the powder spectra.

Table 2. Best fit **g** matrices and corresponding principal g values obtained by the analysis of the single crystal spectra of La-Fe and Ce-Co derivatives.[a]

	La–Fe	Ce–Co		La–Fe	Ce–Co		La–Fe	Ce–Co
g_{XX}	1.893	2.360	g_{XY}	0.458	0.156	g_1	0.734	0.974
g_{YY}	1.231	2.097	g_{YZ}	0.324	−0.120	g_2	2.046	1.68
g_{ZZ}	2.170	0.759	g_{XZ}	0.370	0.138	g_3	2.436	2.63

[a] The reference frame is as follows: X is along the [101] direction, Y is the b direction [010] and Z is perpendicular to both X and Y. Standard deviation for each value: 0.04.

Interestingly, it turns out that irrespective of the choice made, for La–Fe, the lowest g value ($g_1=0.72$) is always oriented very close to the [$\bar{1}$01] direction (max. deviation 9.6°); this is, in turn, close to the Fe−C4 value ($\Delta\theta=13.4°$).

To discriminate among the four different solutions for the orientation of the remaining two principal g values for this system, ligand-field calculations based on the angular overlap model were performed.[31] Use of the angular positions derived from the X-ray structure and of appropriate electronic parameters ($Dq=1800\ cm^{-1}$, $B=350\ cm^{-1}$, $C=1500\ cm^{-1}$, $\zeta=330\ cm^{-1}$, $k=0.76$ $e_\sigma/e_\pi=-0.2$)[32–34] yielded the three principal g values ($g_1=0.738$, $g_2=2.046$, $g_3=2.584$) in quite good agreement with the experimental values. The analysis of the calculated directions, however, displayed large discrepancies for three of the four possible choices obtained from the experimental results. The best agreement was obtained for the choice reported in Table 2, for which the difference of the orientation g_2 principal direction is smaller than 11°, and the remaining calculated principal directions differ from the experimental ones by as much as 30°. As the three other possible experimental choices provided worse agreement with calculated values, this was selected as the actual orientation of the principal axes. It is worth noting here that it was recognised early that the second-coordination sphere of low-spin iron(III) might play a major role in determining the orientation of **g** principal directions in $K_3[Fe(CN)_6]$,[27,33,35] and thus the observed discrepancies should not be regarded as surprising. More recently, a DFT-based study on the Jahn–Teller effect in $[Fe(CN)_6]^{3-}$[36] showed that even minor changes in the structure due to static and/or dynamic Jahn–Teller coupling may lead to large difference in **g** tensor.

With the options suggested by the ligand-field calculations, the two larger components of g values are oriented in a plane slightly tilted (15.3°) with respect to the equatorial plane (Fe-C1-C2-C5-C6). The two components g_1 and g_2 make an angle of 26.7° and 24.6° with Fe−C6 and Fe−C2, respectively. The orientation of the **g** tensor in the molecular frame is shown in Figure 4.

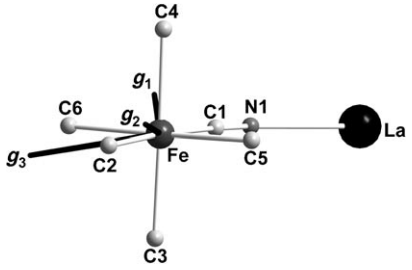

Figure 4. Orientation of the **g** tensor of La–Fe with respect to the coordination sphere of iron and the La-N-C-Fe plane. Each component is proportional to its respective modulus.

The standard analysis of the angular dependence of the g values of a single crystal of Ce–Co (Figure 3, bottom) provided the principal g values and directions which are also re-

ported in Table S1 (Supporting Information). For this system, only two possible combinations yielded a reasonable agreement of principal g values with those obtained from powder spectra. The best agreement (Table 2) is obtained when the principal directions of the g values are oriented close to three planes O3-Ce1-O2 ($g_3=2.62$, $\Delta\theta=4.5°$), O1-Ce1-O6 ($g_2=1.66$, $\Delta\theta=11.3°$), and N1-Ce1-O8 ($g_1=0.974$, $\Delta\theta=0.5°$). This was chosen as the correct orientation of **g** tensor. With respect to the bicapped trigonal prism formed by the Ce coordination sphere (Figure 5, top), it was shown

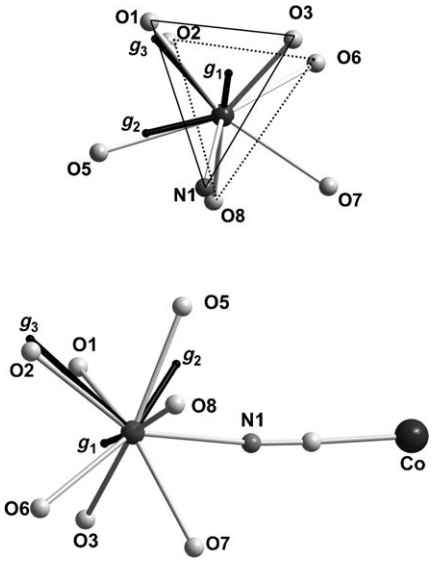

Figure 5. Orientation of the **g** tensor of Ce–Co with respect to the bicapped trigonal prism of the coordination sphere of the Ce centre (upper) and with respect to the Co-C-N-Ce plane (lower). For both figures, each component of the tensor is proportional to its respective modulus.

that g_1 is almost perpendicular to the Ce–N1 direction ($\theta=87.8°$), whereas g_3 is close to the Ce–O2 direction ($\theta=4.56°$). On the other hand, none of the principal directions showed any peculiar relation to the axis of the prism. The corresponding orientation of the **g** tensor in the molecular frame is shown in the lower panel of Figure 5. Quite interestingly, with this choice, the principal direction of g_3 is collinear with that of g_2 for the iron(III) centre.

The single-crystal spectra of Ce–Fe are complicated by the overlap of signals due to the increased number of transitions associated with the two magnetic centres and with monoclinic symmetry. The polycrystalline powder spectra were interpreted with a model which takes into consideration the two effective $S=1/2$ for each of the iron and cerium centres (four states in total) and includes an anisotropic exchange term. The overall pattern of levels was that of a triplet with a weak feature attributed to a singlet–triplet transition.[37]

The main features of the single-crystal spectra confirm the model, as shown by the angular dependence of the resonance fields in the three different planes reported in Figure 6. In particular, the spectra in the XZ plane appa-

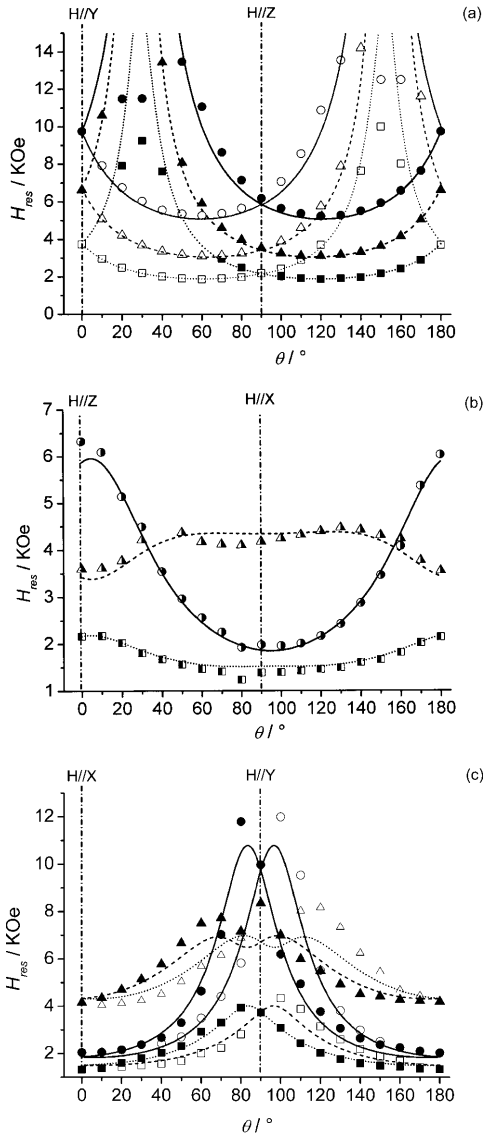

Figure 6. Angular dependence of the resonance position of the single-crystal EPR spectra of Ce–Fe derivatives in three orthogonal planes a) rotation around X; b) rotation around Y; c) rotation around Z and the best simulation obtained with parameters reported in Table 3. For a) and c), full and empty symbols are used to show the resonances attributed to the two inequivalent magnetic centres. Different symbols represent $M=0\rightarrow M=+1$ (triangles), $M=-1\rightarrow M=0$ (circles) and $M=-1\rightarrow M=+1$ (formally forbidden; squares) transitions.

rently correspond to a triplet state, with two allowed and one forbidden transition.[38] Typical spectra are reported in the Supporting Information Figure S1.

The fit of the resonance fields was performed using the spin Hamiltonian [Eq. (1)], in which $S=1$, **H** is the applied magnetic field, and **g** and **D** are the effective Zeeman and zero field splitting tensors of the triplet, respectively:

$$\mathscr{H}=\mu_B\mathbf{S}\cdot\mathbf{g}\cdot\mathbf{H}+\mathbf{S}\cdot\mathbf{D}\cdot\mathbf{S} \quad (1)$$

Assuming that the Zeeman term is dominant, the effective **g** and **D** parameters for each orientation can be estimated

from the spectra as $g_{eff}=2g_eH_0/(H_+ + H_-)$, in which H_+ and H_- are the resonance fields of the $M=0\rightarrow M=\pm 1$ transitions, and as $D'=H_0(H_+ - H_-)/(H_+ + H_-)$, in which $D'=D/(g\mu_B)$ and $H_0=h\nu/g_e\mu_B$.[38] This approach suggests that the **g** and **D** tensors are not collinear, as the extremes for the two calculated parameters do not occur at the same orientation (See Figure S2 in the Supporting Information)

To obtain a reasonable reproduction of the experimental data, we considered the variation of the effective (calculated) g values (Figure S2) in the three orthogonal planes, and in this way we obtained the general $\mathbf{g}^2$ tensor (Table 3)

Table 3. Non-diagonal tensors and corresponding principal values obtained from the best fit of single-crystal EPR spectra of Ce–Fe.[a]

Component	g	D [cm^{-1}]	Principal values
XX	2.123	−0.0824	$g_1=0.165$
YY	0.480	0.0210	$g_2=1.535$
ZZ	1.249	0.0614	$g_3=2.152$
XY	−0.170	0.0	$D_{zz}=-0.084$ cm^{-1}
YZ	0.572	0.0	$D_{yy}=0.063$ cm^{-1}
XZ	−0.032	−0.0153	$D_{xx}=0.021$ cm^{-1}

[a] X, Y, Z are the laboratory axes; x, y, and z the principal directions of D.

to be used in the simulation procedure through standard analysis.[30] Of the four possible combinations, only two gave real principal g values, and their tensor values are related by $g_{XY}=-g_{XY}$, $g_{YZ}=-g_{YZ}$. The second step of the analysis consisted of the simulation[39,40] of the angular dependence in the three planes by including a rhombic zero-field splitting oriented in a general direction, using as starting values the principal values and the orientations obtained by the first-order analysis outlined above. This gave a satisfactory reproduction of the angular dependence of the spectra by using the parameters reported in Table 3.

The obtained principal D values point out a moderately rhombic zero-field splitting ratio ($E/D=-1/6$), in agreement with the low symmetry of the pair.[41] The analysis of the orientation of the **D** tensor in the molecular frame shows that D_{zz} and D_{xx} deviate only by 6.3° and 7.3°, respectively, from the Ce-C-N plane, with D_{yy} being almost perpendicular to it (80.3°). The last direction is also virtually perpendicular (87.7°) to the Ce–Fe direction (Figure 7). On the other hand, none of the principal directions of the chosen **g** tensor are oriented along relevant molecular directions or planes.

Magnetism: The magnetic behaviour of polycrystalline powders of La–Fe, Ce–Co and Ce–Fe has been reported[19,22]. We reanalysed the temperature dependence of χT for La–Fe and Ce–Co (Figure 8) on the basis of the EPR results by using the standard ligand-field arguments described in the Discussion section.

The single-crystal magnetic measurements as a function of the angle and of the temperature are reported in Figures 9 and 10 for Ce–Co and Ce–Fe derivatives, respectively.

As expected, the angular dependence of the susceptibility follows a law of the type $\chi(\theta)=\chi_{ii}\cos^2(\theta)+\chi_{jj}\sin^2(\theta)+$

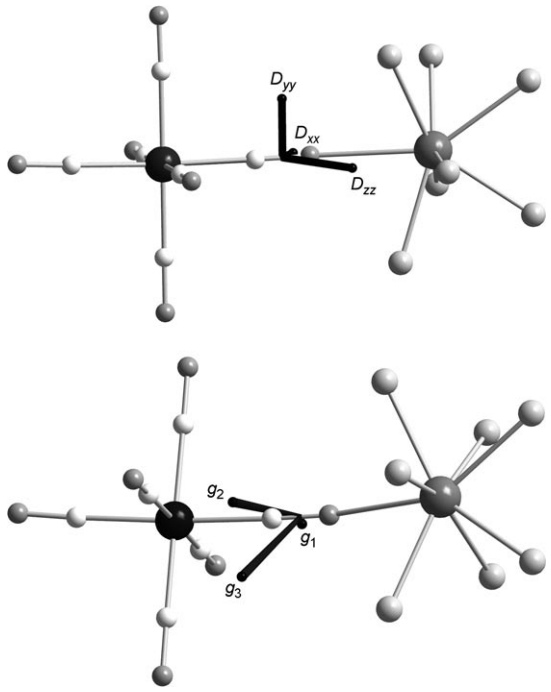

Figure 7. Orientation of the **g** (top) and **D** (bottom) tensors of the pseudo-triplet state of Ce–Fe with respect to the molecular frame. Each component of the two tensors is proportional to its modulus.

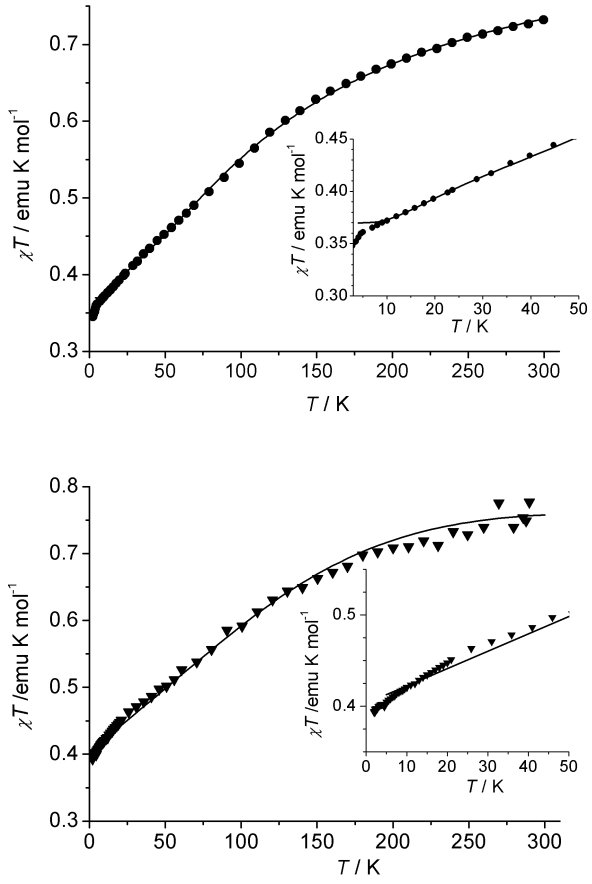

Figure 8. Powder χT versus T plots for Ce–Co (top) and La–Fe (bottom) derivatives, together with best fits obtained by the models described in the text. The insets show the details of the low-temperature regions.

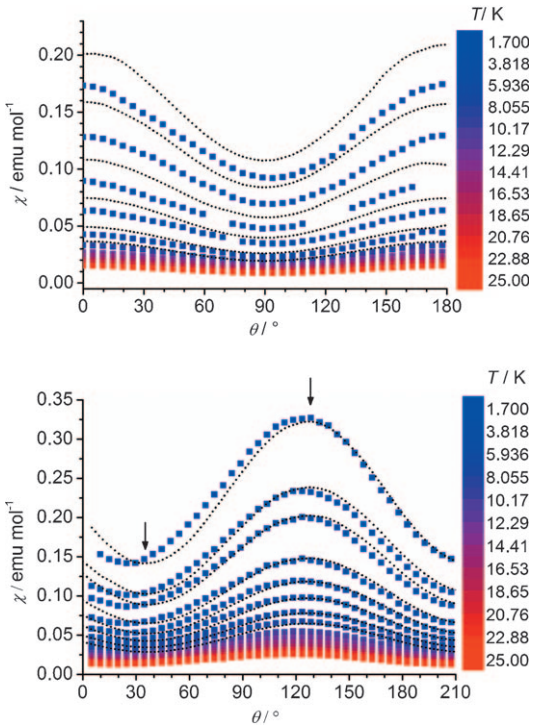

Figure 9. Angular dependence of the magnetic susceptibility as a function of temperature in the *XY* plane (top) and in the *XZ* plane (bottom) for Ce–Co derivative. For the top panel $B \| X$ for $\theta = 0°$ and $B \| Y$ for $\theta = 90°$; for the lower paenl $B \| X$ for $\theta = 0°$ and $B \| Z$ for $\theta = 90°$. The dotted lines represent the angular dependence of χ calculated for an $S = {}^1/_2$ paramagnet with the **g** tensor obtained by EPR study. The arrows show the direction, at the lowest measured temperature, of the two non-symmetry determined crystal magnetic anisotropy axes.

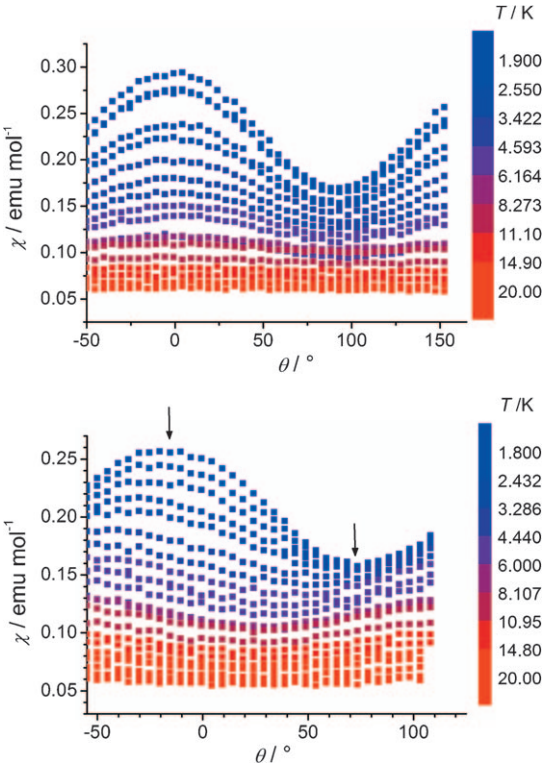

Figure 10. Angular dependence of the magnetic susceptibility as a function of temperature in the *YX* plane (top) and in the ZX plane (bottom) for Ce–Fe. For the top panel $B \| Y$ for $\theta = 0°$ and $B \| X$ for $\theta = 90°$; for the lower one $B \| Z$ for $\theta = 0°$ and $B \| X$ for $\theta = 90°$. The arrows show the direction, at the lowest measured temperature, of the two non-symmetry determined crystal magnetic anisotropy axes.

$2\chi_{ij}\sin(\theta)\cos(\theta)$ for both systems in the two planes in which they were measured.[25] For the Ce–Co derivative at 5 K, the principal axes of crystal susceptibility were found to be oriented at +24.9° (intermediate anisotropy axis), −64.1° (easy axis) from the *X* direction in the *XZ* plane (see arrows in Figure 9, bottom), and the third axis (hard magnetisation) oriented—due to crystal symmetry—along *b*. However, on increasing the temperature above 20 K, the easy and intermediate crystal-axis susceptibility directions rotate smoothly by about 15° at 25 K (Figure S3, left in the Supporting Information).

The rotation of magnetic axes on varying the temperature is even more dramatic for Ce–Fe. In this case, the hard axis, which is oriented at +75° from *X* in the *XZ* plane at 2 K (see arrow in Figure 10, bottom) rotates by about 55° toward *X* when going from 2 K to 15 K (Figure S3, right in the Supporting Information).

Discussion

Electronic structure of the isolated iron(III) centre: The relationship between the principal *g* values of low-spin iron(III) and the composition of the corresponding ground doublet was first pointed out by Griffith[42] and then refined by McGarvey.[32] In this approach the ground doublet is described in the d_{xy}, d_{yz}, d_{xz} basis set as in Equations (2) and (3):

$$\Psi_+ = A|xy,1/2\rangle + B|yz,-1/2\rangle + C|xz,-1/2\rangle \quad (2)$$

$$\Psi_- = -A|\mathrm{xy},-1/2\rangle + B|\mathrm{yz},\ 1/2> -C|xz,1/2\rangle \quad (3)$$

The corresponding *g* values as a function of the orbital reduction factor, *k*, are then given by Equations (4)–(6):

$$g_x = 2(B^2 - A^2 - C^2 - 2kAC) \quad (4)$$

$$g_y = 2(C^2 - B^2 - A^2 - 2kAB) \quad (5)$$

$$g_z = 2(A^2 - C^2 - B^2 - 2kBC) \quad (6)$$

In the case of La–Fe, by using $k = 0.85$,[27] the best fit to the experimental *g* values is obtained for $A^2 = 0.52$, $B^2 = 0.21$, $C^2 = 0.27$. This yields $g_x = -2.434$, $g_y = -2.044$, $g_z = -0.730$. Through this approach it is also possible to obtain the relative strength of the ligand field parameters, Δ and *V*, defined by Equations (7) and (8):

$$\langle d_{xy}|H_{LF}|d_{xy}\rangle = \Delta \quad (7)$$

$$\langle d_{xz}|H_{LF}|d_{xz}\rangle = V/2 - \langle d_{yz}|H_{LF}|d_{yz}\rangle \quad (8)$$

Indeed, Equations (9) and (10) in which ζ is the single-electron spin-orbit coupling constant:[32]

$$\frac{\Delta}{\zeta} = \frac{A(1-A^2) + (B+C)[1-(B+C)^2]}{4ABC} \quad (9)$$

$$\frac{V}{\zeta} = \frac{(A+B+C)(C-B)}{2BC} \quad (10)$$

By substituting the coefficient values obtained above, one obtains $\Delta/\zeta = 0.567$, $V/\zeta = 0.22$, which is in good agreement with data reported in the literature[28,32] and the above-mentioned AOM calculations, indicating that the two excited doublets originating from the splitting of the $^2T_{2g}$ multiplet are at 407.2 and 514.3 cm^{-1}. A reasonable reproduction of the χT versus T behaviour of La–Fe (Figure 8) was obtained by using this energy pattern, thus confirming the reliability of the parameters used in the AOM calculations. We can thus conclude that the ground doublet of the iron(III) results from considerable contribution of all the three d (t_{2g}) orbitals with a major contribution from d_{xy}. Furthermore, magnetic and EPR data point to an energy of the first two excited doublets at around 400 and 500 cm^{-1}, respectively (Figure 11, left panel).[35]

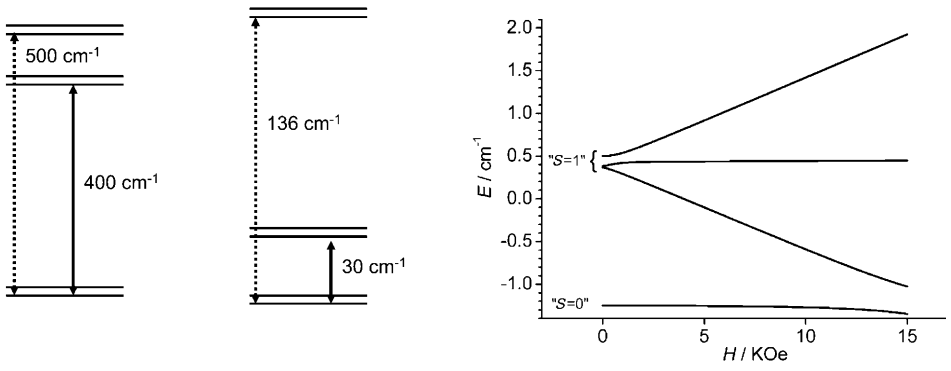

Figure 11. Energy pattern of the lowest lying levels obtained by the analysis of single-crystal magnetic and EPR data for La–Fe (left), Ce–Co (centre) and Ce–Fe (right). For Ce–Fe, the dependence on the magnetic field applied along the X axis is also reported. Relative energies for the three derivatives are not in scale.

Electronic structure of the isolated cerium(III) centre: The relationship between g values of Ce–Co and the composition of its ground state can be obtained by assuming that the energy of the excited $^2F_{7/2}$ is high enough to justify using only the components of the ground $^2F_{5/2}$ multiplet. As a first approximation, we can consider the geometry around the cerium(III) centre to be orthorhombic. In this case, the principal axes are symmetry-determined and the ground doublet will have the general form given in Equation (11), in which the wave functions are labelled using the M_J components and only states differing by $\Delta M_J = \pm 2$ contribute to each doublet:

$$\Phi_{\pm} = a|\pm 5/2\rangle + b|\pm 1/2\rangle + c|\mp 3/2\rangle \quad (11)$$

Linear combinations, including all of the 6 M_J components, should be included in the general low-symmetry case. Use of Equation (11) results in the following expressions for the corresponding g_{eff} values[29,43] [Eq.s (12)–(14)), in which the g_J value is given by the Landé formula [Eq. (15)] and corresponds to 6/7:

$$g_x = g_J(3a^2 + 2ac\sqrt{5} + 4bc\sqrt{2}) \quad (12)$$

$$g_y = g_J(3a^2 + 2ac\sqrt{5} - 4bc\sqrt{2}) \quad (13)$$

$$g_z = g_J(5a^2 + b^2 - 3c^2) \quad (14)$$

$$g_J = 1 + \frac{J(J+1) + S(S+1) - L(L+1)}{2J(J+1)} \quad (15)$$

The best fit to the experimental data is obtained for a ground Kramers doublet corresponding to $0.7495|\pm 5/2\rangle - 0.6573|\pm 1/2\rangle - 0.0783|\mp 3/2\rangle$ and yielding calculated values which agree with the observed ones within 12% (calculated values $g_x = 0.97$, $g_y = 1.47$, $g_z = 2.76$). The observed discrepancy can be attributed both to a small amount of mixing of the $^2F_{7/2}$ state in the ground doublet and to the assumption of orthorhombic symmetry.[23,29]

This allows us to obtain the description of the ground state in the f orbital representation by transforming the wavefunction given by Equation (11) in the $|J,M_J\rangle$ basis to that of $|L=3, S=1/2, M_L, M_S\rangle = |M_L, M_S\rangle$, by use of Clebsch–Gordan coefficients.[44] This analysis leads to a description of the ground state with the following composition: 18.5% 4fσ ($|M_L=0, M_S=\pm 1/2\rangle$), 25% 4fπ ($|M_L=\pm 1, M_S=\pm 1/2\rangle$), 8.4% 4fδ ($|M_L=\pm 2, M_S=\pm 1/2\rangle$), 48.1% 4fϕ ($|M_L=\pm 3, M_S=\mp 1/2\rangle$).

We used the information obtained by single-crystal EPR measurements to simulate the angular dependence of the susceptibility calculated on the basis of the Curie law for a doublet with the **g** tensor for which we already know the absolute values and orientations. This approach provides a good reproduction of the experimental data in terms of the orientation of principal crystalline susceptibilities and relative anisotropy up to 20 K, whereas the quantitative agreement is somewhat poorer (Figure 9). Moreover, above 20 K, these results suggest the presence of a relatively low-lying excited doublet, as indicated by the fit of the powder measurements. In fact, a good fit of the latter could be performed by applying the Van Vleck equation to this system, fixing values obtained by EPR ex-

periments for the ground doublet and leaving average g values for the two excited doublets and the energy differences between the three doublets as free parameters[45] [Eq. (16)]:

$$\chi T = \frac{N\mu_B{}^2}{4k}\frac{\sum_i (g_{\mathrm{eff,ave}})_i^2 \exp(-E_i^0/kT)}{\sum_i \exp(-E_i^0/kT)} \quad (16)$$

The best fit curve obtained by this procedure is reported in Figure 8 and yields $g_{\mathrm{eff,ave}}$ values of 2.5 and 4.2 for two doublets located at 30 and 136 cm^{-1} above the ground state, respectively. The obtained energy pattern (Figure 11, central panel) is in agreement with that reported for Ce^{3+} chloride derivatives.[23,46]

The smooth rotation of the principal direction of the crystalline magnetic susceptibility observed above 20 K can then be explained by assuming a progressive population of an excited doublet, in which the principal directions and magnitude of susceptibilities are different with respect to those of the ground state. Such a phenomenon has already been seen in one of the few reported examples of single-crystal magnetic measurements on a cerium(III) salt.[47] As the use of Equation (11) implies that the principal axes of the three Kramers doublets are fixed, the observed rotation of magnetic axes with temperature confirms that the assumption of orthorhombic symmetry is not completely justified, and each of the two wavefunctions is a linear combination of all the M_J components.

The Ce–Fe coupled species: Having defined the electronic and magnetic structures of the two paramagnetic centres in the uncoupled systems, that is, Ce–Co and La–Fe, we can now discuss the results obtained for the coupled species Ce–Fe, the analysis of which is much more complex. The single-crystal EPR spectra were interpreted (see above) as originating from a triplet state, with anisotropic and misaligned **D** and **g** tensors. However, this interpretation does not provide us with much information concerning the exchange interaction between the two centres. We then tried to rationalise the observed properties at the lowest temperature, by correlating the spin Hamiltonian parameters of the triplet states with those of the two lowest Kramer doublets of cerium(III) and iron(III). In this case the spin Hamiltonian is given by Equation (17):[24]

$$\mathscr{H} = \mu_B(\mathbf{S_1}\cdot\mathbf{g_1} + \mathbf{S_2}\cdot\mathbf{g_2})\cdot\mathbf{H} + \mathbf{S_1}\cdot\mathbf{J_{12}}\cdot\mathbf{S_2} \quad (17)$$

In Equation (17), the first two terms are the Zeeman terms of the individual ions, which we derived by the analysis of the EPR of Ce–Co and La–Fe, and the third term describes the interaction. J_{12} is a general 3×3 dyadic of both dipolar and exchange origin that can be decomposed into three terms: isotropic (J), anisotropic(D_{12}), and antisymmetric ($\mathbf{d_{12}}$) [Eq. (18)]:

$$\mathbf{S_1}\cdot\mathbf{J_{12}}\cdot\mathbf{S_2} = J\mathbf{S_1}\cdot\mathbf{S_2} + \mathbf{S_1}\cdot\mathbf{D_{12}}\cdot\mathbf{S_2} + \mathbf{d_{12}}\cdot\mathbf{S_1}\times\mathbf{S_2} \quad (18)$$

While the exchange contribution cannot be evaluated in a straightforward manner, the dipolar contribution to each term is easily calculated by means of the point dipolar approximation by using the crystal structure coordinates and the **g** tensors of Ce–Co and La–Fe obtained by the single crystal EPR spectra. This yields principal values $J^{\mathrm{dip}} = -9\times10^{-5}$ cm^{-1}, $D^{\mathrm{dip}} = 0.0213$ cm^{-1}, $E^{\mathrm{dip}}/D^{\mathrm{dip}} = -0.16$ which are much smaller than the experimentally determined values for the **D** tensor of the triplet state, as shown in Table 4. Furthermore, due to the noncollinearity of the $\mathbf{g_i}$ tensors, the principal component of the calculated dipolar tensor is not aligned along the line connecting the two spins and points in a completely general direction (Table 4). The antisymmetric component of the dipolar interaction is calculated to be $d^x = 1.70\times10^{-3}$, $d^y = 6.01\times10^{-4}$, $d^z = -3.42\times10^{-3}$ cm^{-1}. This is indicative of the possibility that the antisymmetric contribution can be of comparable magnitude to the anisotropic one.

Table 4. Direction cosines of the principal axes, x, y and z of the experimentally determined **D** tensor and of the calculated dipolar tensor.[a,b]

	D^{xx}_{tripl}	D^{yy}_{tripl}	D^{zz}_{tripl}	D^{xx}_{dip}	D^{yy}_{dip}	D^{zz}_{dip}	Ce–Fe direction
$\cos\alpha$	−0.1046	0.0	0.9945	0.4465	−0.2418	−0.8615	0.8340
$\cos\beta$	0.0	1.0	0.0	0.8770	−0.0729	0.4750	0.5367
$\cos\gamma$	0.9945	0.0	−0.1046	0.1776	0.9676	−0.1796	0.1277
values	0.021	0.063	−0.084	0.0105	0.0037	−0.0142	

[a] All the cosines are expressed in the XYZ laboratory frame (α is the angle with X, β with Y and γ with Z). [b] In the last line the corresponding values [in cm^{-1}] are listed for the sake of clarity.

It has to be considered that the effect of the last term of Equation (18) on the energy pattern of the resulting coupled state has been shown[48,49] to be equivalent to that of an additional contribution to the global ZFS, of magnitude $D_{\mathrm{as}} \approx d^2J$ (in which d denotes the modulus of $\mathbf{d_{12}}$). For a system with quenched orbital contribution d is usually estimated on the basis of the Moriya[50] approximation, which considers d to be proportional to $(\Delta g/g)J$. The situation is, however, more complex for systems with a relevant orbital contribution, for which Levy and Stevens[51,52] have shown that the antisymmetric term can in principle be of the same order of magnitude as the anisotropic and isotropic terms. On these bases, it is not possible to attribute a predominant importance to one of the two possible contributions to the zero-field splitting of the pseudo-triplet state which is responsible for the observed EPR spectrum.

With all these considerations in mind, we tried to fit the experimental pseudo-triplet EPR spectra also using a model based on Equation (17) by fixing the individual **g** tensors to those determined by the EPR of La–Fe and Ce–Co and using the nine parameters of $\mathbf{J_{12}}$ as unknown. For the sake of simplicity, we restricted ourselves to the analysis in the XZ plane, in which the two molecules related by the C_2 axis are equivalent. The first important result which was obtained from this simulation concerns the magnitude of the isotropic exchange, J. A lower limit of 1.3 cm^{-1} can be estab-

lished, since below this value a transition between the pseudo-singlet and the pseudo-triplet should become visible in the high-field region. The second relevant result concerns the effect of the antisymmetric term on the spectra. Test simulation showed, in agreement with the considerations discussed above, that it might play a relevant role, and in particular d^x and d^z components ranging between 0.5 and 1.0 cm^{-1} should be included. A good reproduction of the angular dependence of the spectrum was then obtained with the following set of parameters: $|J|>1.3\ cm^{-1}$, $D_{xx}=0.02\ cm^{-1}$, $D_{yy}=0.02\ cm^{-1}$, $D_{zz}=-0.04\ cm^{-1}$, $d^z=0.75\ cm^{-1}$, $d^x=0.5\ cm^{-1}$, $d^y=0$ (Figure S5). This set of values indicates that the antisymmetric part of the coupling tensor is of comparable magnitude to the isotropic one and larger than the anisotropic one, as may be expected for a system containing two centres with unquenched orbital momentum. The resulting low-energy pattern of the states of the Ce-Fe derivative, as well as their dependence on applied magnetic field along the X direction is reported in the right panel of Figure 11, in which the pseudo-singlet and pseudo-triplet character of the states arising from these parameters is shown.

A further degree of complexity is introduced by the analysis of the single-crystal magnetic data, and, in particular, by the strong temperature dependence of the anisotropy directions observed in the XZ plane. This can be qualitatively explained by considering that the coupling between the two centres is antiferromagnetic. In this assumption, at low temperatures, the ground state is a weakly magnetised state, the resulting **g** tensor of which will be equal to $(g_1-g_2)/2$, whereas, upon increasing the temperature, the magnetic properties of the complex change towards the average of the two magnetic centres, and depend on $(g_1+g_2)/2$. Given the large anisotropy and misalignment of the two **g** tensors, this process results in a rotation of the anisotropy axes upon increasing the temperature. A similar behaviour has been recently reported for a Mn^{III}-based single-chain magnet[6c] and can be considered typical for weakly antiferromagnetically coupled systems whose interacting centres present a misaligned anisotropy axis. By considering the two **g** tensors experimentally determined by EPR and assuming a value of the isotropic constant of $J_{AF}=3.1\ cm^{-1}$ a rotation of 13° on going from 2 K to 15 K is indeed obtained (Figure 12). Furthermore, this value of the isotropic part of the exchange coupling tensor is able to reproduce the experimentally observed presence of a maximum at 2.8 K in the M versus T plot only at some orientations in the XY plane (inset of Figure 12). It is worth noting that not only the assumption of a simple triplet state, but also the use of ferromagnetic coupling fails in reproducing these experimental findings. The single-crystal magnetic data can then be considered as a definitive proof of antiferromagnetic coupling between the two centres, a piece of information which could not be gained by EPR spectroscopy.

Notwithstanding this success, it has to be said that even this model is not able to reproduce some relevant features of the magnetic data. As an example, the calculated anisotropy in the XY plane is of opposite sign with respect to the experimental value (Figure S6 in the Supporting Information).

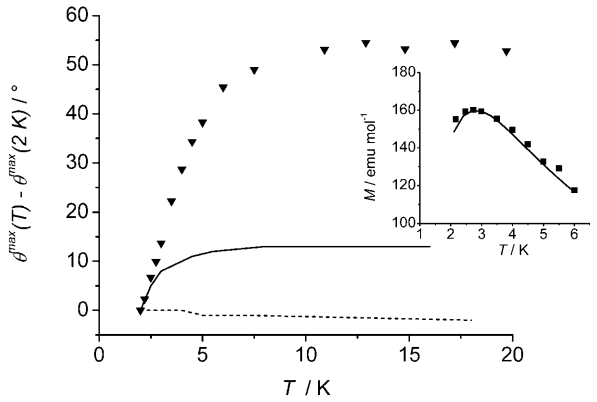

Figure 12. Experimentally observed rotation of the anisotropy axis of Ce–Fe with respect to the orientation at 2 K and calculated behaviour assuming antiferromagnetic (continuous line) and ferromagnetic (dashed line) exchange coupling of 3.1 cm^{-1}. In the inset, a comparison between the experimental and calculated M versus T in the X direction using $J_{AF}=3.1\ cm^{-1}$ and the **g** tensors derived for La–Fe and Ce–Co is reported.

This analysis suggests an inadequacy of the models used to reproduce single-crystal EPR data, which we attribute to the presence of low-lying excited states that escape EPR detection and which contribute to the strongly temperature-dependent rotation of the principal anisotropy axis in the XZ plane. On the basis of the energy pattern obtained for cerium(III) and iron(III), it can be argued that these levels arise as a consequence of the coupling of the ground iron(III) doublet with at least the two lowest lying doublets of the cerium(III) centre. If the coupling is weak and—as has to be expected—strongly anisotropic,[48] each of these couplings results in four weakly split levels, for a total of eight states, the energies of which rapidly change with the direction of the applied field. It is quite evident that the inclusion of these additional levels would result in an excessive number of parameters to be determined through a fitting of the magnetic and EPR data.

Conclusion

In this paper we reported a detailed single-crystal EPR and magnetic studies of a homologous series of complexes of the type Ln–M (Ln = La, Ce; M = Fe, Co), with the aim of elucidating the relative importance of exchange and anisotropy contributions, as well as to test the validity of the diamagnetic substitution approach at a quantitative level. We were able to obtain a detailed picture of the low-lying levels of Ce^{III} and Fe^{III} centres through the combined use of single-crystal EPR and magnetic susceptibility data. We showed that classical ligand-field theory can be of great help in rationalising the energies of the low-lying levels of both transition metal and rare earth ions.

The combined analysis of single-crystal EPR and magnetic data of the coupled system Ce–Fe confirmed the great

complexity of the interactions involving rare-earth elements. Although some uncertainty remains, it is clear that the interaction involving the lowest lying spin levels requires the introduction of the isotropic, anisotropic and antisymmetric terms. Because of such complexity, the usual approximation bound to the diamagnetic substitution must be regarded even more critically, because it can only record a very highly mediated response from many different interaction pathways.

We feel that showing the need for introducing the antisymmetric exchange is an important step in molecular magnetism, because it may open important perspectives and clarify several cases, in which it has been suggested to be present. Even if the possibility of developing structural correlations with this parameter appears to be difficult at this stage, we feel this last point to be of particular importance, since the role of the antisymmetric exchange is often underestimated, even in systems containing centres with unquenched orbital momentum. Clearly more experimental and theoretical work is needed on this point, focusing on the simplest possible systems. In particular, the sources of the problems encountered in this study are the weakness of the isotropic exchange coupling and the presence of low lying excited states in the cerium(III) centre, which produce a relatively large number of populated states with pronounced anisotropy that are impossible to deal with at our current level of understanding. This is well evidenced by the somehow conflicting results obtained by the analysis of single-crystal EPR and magnetic data of Ce–Fe. The next investigation should then focus on systems with stronger exchange interactions and a larger separation between the ground and first excited doublet of the lanthanide ion.

We can then conclude that this study once again points out the absolute necessity of detailed single-crystal analysis to obtain meaningful, but still incomplete information concerning the anisotropic properties of exchange coupled pairs containing orbitally nondegenerate ions. This is usually not the case, and for many such systems reported in literature, the parameters are derived by studies of powder samples.[53] We believe that this procedure might be justified only by the absence of suitable single crystals, but even in that case one should be aware that the obtained results should be regarded with much caution. We have shown here that complete single-crystal studies and analysis are difficult tasks to be performed, but we feel that trying to unravel suitable models to design new magnetic materials requires this kind of effort.

Experimental Section

The compounds were prepared as previously reported.[22]

Powder X-band spectra of **1** were recorded on a Bruker ESP300 spectrometer equipped with an Oxford ESR900 cryostat for low-temperature studies. Single-crystal X-band EPR spectra were recorded on a Varian E9 line spectrometer equipped with an Oxford Instrument cryostat and a manual goniometer for variable orientation studies. Due to the visual procedure of alignment, the estimated error in this kind of measurement is about $\pm 5°$. For each spectrometer, resonance fields were calibrated by independently measuring a small amount of 2,2-diphenyl-1-picrylhydrazyl (DPPH; $g = 2.0037$). Magnetic measurements were performed using a Cryogenic S600 SQUID magnetometer. Single-crystal experiments ($m_{CeCo} = 13.5$ mg, $m_{CeFe} = 0.6$ mg) were performed in steps of 5° by using an adapted Quantum Design rotator with estimated precision of 1°. Single crystals used for anisotropic EPR and magnetic measurements were oriented by using a Cad4 Nonius four circles diffractometer with $Mo_{K\alpha}$ radiation.

Acknowledgement

This work was financially supported by EU through contract NMP3-CT-2005-515767 (NoE Magmanet). R. Sessoli is kindly acknowledged for her critical reading of the manuscript and useful suggestions.

[1] *Magnetism: Molecules to Materials, Vol. I–V* (Eds.: J. S. Miller, M. Drillon), Wiley-VCH, Weinheim, **2001–2004**.
[2] *Magnetic Molecular Materials, NATO ASI Ser. E 198* (Eds.: D. Gatteschi, O. Kahn, J. S. Miller, F. Palacio), Plenum, Dordrecht, **1991**.
[3] a) J. M. Manriquez, G. T. Yee, R. S. McLean, A. J. Epstein, J. S. Miller, *Science* **1991**, *252*, 1415; b) S. Ferlay, T. Mallah, R. Ouahes, P. Veillet, M. Verdaguer, *Nature* **1995**, *378*, 701.
[4] a) D. Gatteschi, R. Sessoli, J. Villain, *Molecular Nanomagnets*, Oxford University Press, Oxford, **2006**; b) D. Gatteschi, R. Sessoli, *Angew. Chem.* **2003**, *115*, 278; *Angew. Chem. Int. Ed.* **2003**, *42*, 268.
[5] a) R. Sessoli, D. Gatteschi, A. Caneschi, M. A. Novak, *Nature* **1993**, *365*, 141; b) L. Thomas, F. Lionti, R. Ballou, D. Gatteschi, R. Sessoli, B. Barbara, *Nature* **1996**, *383*, 145; c) J. R. Friedman, M. P. Sarachik, J. Tejada, R. Ziolo, *Phys. Rev. Lett.* **1996**, *76*, 3830.
[6] a) A. Caneschi, D. Gatteschi, N. Lalioti, C. Sangregorio, R. Sessoli, G. Venturi, A. Vindigni, A. Rettori, M. G. Pini, M. A. Novak, *Angew. Chem.* **2001**, *113*, 1810; *Angew. Chem. Int. Ed.* **2001**, *40*, 1760; b) R. Clerac, H. Miyasaka, M. Yamashita, C. Coulon, *J. Am. Chem. Soc.* **2002**, *124*, 12837; c) K. Bernot, J. Luzon, R. Sessoli, A. Vindigni, J. Thion, S. Richeter, D. Leclercq, J. Larionova, A. van der Lee, *J. Am. Chem. Soc.* **2008**, *130*, 1619; d) R. Lescouëzec, J. Vaissermann, C. Ruiz-Pérez, F. Lloret, R. Carrasco, M. Julve, M. Verdaguer, Y. Dromzee, D. Gatteschi, W. Wernsdorfer, *Angew. Chem.* **2003**, *115*, 1521; *Angew. Chem. Int. Ed.* **2003**, *42*, 1483; e) E. Pardo, R. Ruiz-Garcia, F. Lloret, J. Faus, M. Julve, Y. Journaux, F. Delgado, C. Ruiz-Perez, *Adv. Mater.* **2004**, *16*, 1597; f) T. F. Liu, D. Fu, S. Gao, Y. Z. Zhang, H. L. Sun, G. Su, Y. J. Liu, *J. Am. Chem. Soc.* **2003**, *125*, 13976; g) T. Kajiwara, M. Nakano, Y. Kaneko, S. Takaishi, T. Ito, M. Yamashita, A. Igashira-Kamiyama, H. Nojiri, Y. Ono, N. Kojima, *J. Am. Chem. Soc.* **2005**, *127*, 10150; h) Y. L. Bai, J. Tao, W. Wernsdorfer, O. Sato, R. B. Huang, L. S. Zheng, *J. Am. Chem. Soc.* **2006**, *128*, 16428.
[7] a) F. Cinti, A. Rettori, M. G. Pini, M. Mariani, E. Micotti, A. Lascialfari, N. Papinutto, A. Amato, A. Caneschi, D. Gatteschi, M. Affronte, *Phys. Rev. Lett.* **2008**, *100*, 057203; b) R. Andrés, M. Brissard, M. Gruselle, C. Train, J. Vaissermann, B. Malézieux, J.-P. Jamet, M. Verdaguer, *Inorg. Chem.* **2001**, *40*, 4633.
[8] a) A. Bleuzen, C. Lomenech, V. Escax, F. Villain, F. Varret, Ch. Cartier dit Moulin, M. Verdaguer, *J. Am. Chem. Soc.* **2000**, *122*, 6648; b) O. Sato, T. Iyoda, A. Fujishima, K. Hashimoto, *Science* **1996**, *272*, 704;
[9] a) J. Villain, F. Hartmann-Boutron, R. Sessoli, A. Rettori, *Europhys. Lett.* **1994**, *27*, 159; b) R. J. Glauber, *J. Math. Phys.* **1963**, *4*, 294.
[10] J. S. Griffith, *The Theory of Transition-Metal Ions*, Cambridge University Press, Cambridge, **1964**.
[11] a) C. Benelli, D. Gatteschi, *Chem. Rev.* **2002**, *102*, 2369; b) H. U. Guedel, A. Furrer, H. Blank, *Inorg. Chem.* **1990**, *29*, 4081.
[12] a) C. Benelli, A. Caneschi, D. Gatteschi, R. Sessoli, *Adv. Mater.* **1992**, *4*, 504; b) C. Benelli, A. Caneschi, D. Gatteschi, R. Sessoli, *Inorg. Chem.* **1993**, *32*, 4797; c) F. Prins, E. Pasca, L. J. de Jongh, H.

Kooijman, A. L. Spek, S. Tanase, *Angew. Chem.* **2007**, *119*, 6193; *Angew. Chem. Int. Ed.* **2007**, *46*, 6081; d) A. Figuerola, C. Diaz, J. Ribas, V. Tangoulis, C. Sangregorio, D. Gatteschi, M. Maestro, J. Mahía, *Inorg. Chem.* **2003**, *42*, 5274.

[13] a) S. Osa, T. Kido, N. Matsumoto, N. Re, A. Pochaba, J. Mrozinski, *J. Am. Chem. Soc.* **2004**, *126*, 420; b) A. Mishra, W. Wernsdorfer, K. A. Abboud, G. Christou, *J. Am. Chem. Soc.* **2004**, *126*, 15648; c) A. Mishra, W. Wernsdorfer, S. Parsons, G. Christou, E. K. Brechin, *Chem. Commun.* **2005**, 2086; d) C. M. Zaleski, E. C. Depperman, J. W. Kampf, M. L. Kirk, V. Pecoraro, *Angew. Chem.* **2004**, *116*, 4002; *Angew. Chem. Int. Ed.* **2004**, *43*, 3912; e) C. Aronica, G. Pilet, G. Chastanet, W. Wernsdorfer, J.-P. Jacquot, D. Luneau, *Angew. Chem.* **2006**, *118*, 4775; *Angew. Chem. Int. Ed.* **2006**, *45*, 4659; f) M. Ferbinteanu, T. Kajiwara, K.-Y. Choi, H. Nojiri, A. Nakamoto, N. Kojima, F. Cimpoesu, Y. Fujimura, S. Takaishi, M. Yamashita, *J. Am. Chem. Soc.* **2006**, *128*, 9008; g) F. Pointillart, K. Bernot, R. Sessoli, D. Gatteschi, *Chem. Eur. J.* **2007**, *13*, 1602; h) F. Mori, T. Nyui, T. Ishida, T. Nogami, K.-Y. Choi, H. Nojiri, *J. Am. Chem. Soc.* **2006**, *128*, 1440.

[14] a) L. Bogani, C. Sangregorio, R. Sessoli, D. Gatteschi, *Angew. Chem.* **2005**, *117*, 5967; *Angew. Chem. Int. Ed.* **2005**, *44*, 5817; b) K. Bernot, L. Bogani, A. Caneschi, D. Gatteschi, R. Sessoli, *J. Am. Chem. Soc.* **2006**, *128*, 7947.

[15] L. Bogani, D. Gatteschi, R. Sessoli, A. Vindigni, *J. Mater. Chem.* **2008**, *18*, 4750.

[16] P. M. Levy, *Phys. Rev.* **1964**, *135*, A155; P. M. Levy, *Phys. Rev.* **1966**, *147*, 311.

[17] a) J. P. Costes, F. Dahan, A. Dupuis, J.-P. Laurent, *Chem. Eur. J.* **1998**, *4*, 1616; b) M. L. Kahn, J. P. Sutter, S. Golhen, P. Guionneau, L. Ouahab, O. Kahn, D. Chasseau, *J. Am. Chem. Soc.* **2000**, *122*, 3413; c) M. L. Kahn, C. Mathoniere, O. Kahn, *Inorg. Chem.* **1999**, *38*, 3692; d) M. L. Kahn, P. Lecante, M. Verelst, C. Mathonière, O. Kahn, *Chem. Mater.* **2000**, *12*, 3073; e) M. L. Kahn, R. Ballou, P. Porcher, O. Kahn, J.-P. Sutter, *Chem. Eur. J.* **2002**, *8*, 525; f) A. Caneschi, A. Dei, D. Gatteschi, L. Sorace, S. Poussereau, *Dalton Trans.* **2004**, 1048.

[18] a) T. Shiga, N. Ito, A. Hidaka, H. Okawa, S. Kitagawa, M. Ohba, *Inorg. Chem.* **2007**, *46*, 3492;b) C. A. Barta, S. R. Bayly, P. W. Read, B. O. Patrick, R. C. Thompson, C. Orvig, *Inorg. Chem.* **2008**, *47*, 2280; c) C. A. Barta, S. R. Bayly, P. W. Read, B. O. Patrick, R. C. Thompson, C. Orvig, *Inorg. Chem.* **2008**, *47*, 2294; d) T. Yamaguchi, Y. Sunatsuki, H. Ishida, M. Kojima, H. Akashi, N. Re, N. Matsumoto, A. Pochaba J. Mrozinski, *Bull. Chem. Soc. Jpn.* **2008**, *81*, 598.

[19] A. Figuerola, V. Tangoulis, Y. Sanakis, *Chem. Phys.* **2007**, *334*, 204.

[20] a) V. Tangoulis, A. Figuerola, *Chem. Phys.* **2007**, *340*, 293; b) V. Tangoulis, A. Figuerola, J. Ribas, C. Diaz, *Chem. Phys.* **2007**, *336*, 74.

[21] a) T. Afrati, C. Dendrinou-Samara, C. Raptopoulou, A. Terzis, V. Tangoulis, D. P. Kessissoglou, *Dalton Trans.* **2007**, 5156; b) J. Yoon, E. I. Solomon, *Coord. Chem. Rev.* **2007**, *251*, 379; c) M. I. Belinsky, *Inorg. Chem.* **2006**, *45*, 9096; d) B. Tsukerblat, A. Tarantul, A. Müller, *J. Chem. Phys.* **2006**, *125*, 054714; e) A. Tarantul, B. Tsukerblat, A. Müller, *Chem. Phys. Lett.* **2006**, *428*, 361; f) S. Bertaina, S. Gambarelli, T. Mitra, B. Tsukerblat, A. Müller, B. Barbara, *Nature* **2008**, *453*, 203.

[22] A. Figuerola, C. Diaz, J. Ribas, V. Tangoulis, F. Lloret, J. Mahia, M. Maestro, *Inorg. Chem.* **2003**, *42*, 641.

[23] A. Abragam, B. Bleaney, *Electron Paramagnetic Resonance of Transition Ion*s, Dover, New York, **1986**.

[24] A. Bencini, D. Gatteschi, *EPR of Exchange Coupled Systems*, Springer, Berlin, **1990**.

[25] a) S. Mitra in *Transition Metal Chemistry, Vol. 7*, Marcel Dekker, New York, **1972**, pp. 183–337; b) S. Mitra, *Prog. Inorg. Chem.* **1977**, *22*, 309.

[26] M. G. B. Drew, *Coord. Chem. Rev.* **1977**, *24*, 179.

[27] B. N. Figgis, M. Gerloch, R. Mason, *Proc. R. Soc. London Ser. A* **1969**, *309*, 91.

[28] a) J. M. Baker, B. Bleaney, K. D. Bowers, *Proc. Phys. Soc. London Sect. B* **1956**, *69*, 1205; b) J.-P. Willems, M. P. J. W. Clephas, E. de Boer, *Mol. Phys.* **1993**, *80*, 607.

[29] H. R. Lewis, *J. Appl. Phys.* **1966**, *37*, 739.

[30] D. S. Schonland, *Proc. Phys. Soc. London Sect. A* **1958**, *73*, 788.

[31] A. Bencini, I. Ciofini, M. G. Uytterhoeven, *Inorg. Chim. Acta* **1998**, *274*, 90.

[32] B. R. McGarvey, *Coord. Chem. Rev.* **1998**, *170*, 75.

[33] L. Duelund, H. Toftlund, *Spectrochim. Acta A* **2000**, *56*, 331.

[34] a) J. Baker, B. N. Figgis, *Aust. J. Chem.* **1982**, *35*, 265; b) J. Baker, B. N. Figgis, *J. Chem. Soc. Dalton Trans.* **1975**, 598.

[35] a) B. N. Figgis, *Trans. Farad. Soc.* **1961**, *57*, 198; b) B. N. Figgis, *Trans. Farad. Soc.* **1961**, *57*, 204.

[36] M. Atanasov, P. Comba, C. A. Daul, A. Hauser, *J. Phys. Chem. A* **2007**, *111*, 9145.

[37] The analysis of the spectra suggested $J<2\ cm^{-1}$, with $D=0.06\ cm^{-1}$ ($D=J_{zz}-[J_{xx}+J_{yy}]/2$)and $E=0.05\ cm^{-1}$($E=[J_{xx}-J_{yy}]/2$) However, this set contrasts with the usual formalism which constrains $E/D<1/3$: a standard formulation would be $D=0.105\ cm^{-1}$ $E/D=0.047$.

[38] J. A. Weil, J. R. Bolton, J. E. Wertz, *Electron Paramagnetic Resonance: Elementary Theory and Practical Applications*, Wiley-Interscience, New York, **2001**.

[39] a) S. Mossin, H. Weihe, A.-L. Barra, *J. Am. Chem. Soc.* **2002**, *124*, 8764; b) C. J. H. Jacobsen, E. Pedersen, J. Villadsen, H. Weihe, *Inorg. Chem.* **1993**, *32*, 1216.

[40] S. Stoll, A. Schweiger, *J. Magn. Reson.* **2006**, *178*, 42.

[41] We stress here that with this set of parameters we were able to satisfactorily reproduce both the perpendicular- and parallel-polarisation powder X-Band spectra reported in reference [19] (see Figure S4 in the Supporting Information).

[42] J. S. Griffith, *Nature* **1957**, *180*, 30.

[43] R. M. Golding, T. Singhasuwich, W. C. Tennant, *Mol. Phys.* **1977**, *34*, 1343.

[44] V. Mehta, D. Gourier, *J. Phys. Condens. Matter* **2001**, *13*, 4567.

[45] E. A. Boudreaux, L. N. Mulay, *Theory and Applications of Molecular Paramagnetism*, Wiley, New York, **1976**.

[46] a) K. H. Hellwege, E. Orlich, G. Schaak, *Phys. Kondens. Mater.* **1965**, *4*, 196; b) R. C. Mikkelson, H. J. Stapleton, *Phys. Rev.* **1965**, *140*, A1968; c) C. A. Hutchison, E. Wong, *J. Chem. Phys.* **1958**, *29*, 754.

[47] A. Mookerji, *Indian J. Phys.* **1949**, *23*, 217.

[48] A. Bencini, D. Gatteschi, C. Zanchini, *Mol. Phys.* **1985**, *56*, 97.

[49] a) J. Choukroun, J.-L. Richard, A. Stepanov, *Phys. Rev. Lett.* **2001**, *87*, 127207; b) S. Bertaina, V. A. Pashchenko, A. Stepanov, T. Masuda, K. Uchinokura, *Phys. Rev. Lett.* **2004**, *92*, 057203.

[50] T. Moriya, *Phys. Rev.* **1960**, *120*, 91.

[51] K. W. H. Stevens, *Rev. Mod. Phys.* **1953**, *25*, 166.

[52] P. M. Levy, *Phys. Rev. Lett.* **1968**, *20*, 1366; P. M. Levy, *Phys. Rev.* **1969**, *177*, 509.

[53] see, for example, Y. Ouyang, W. Zhang, N. Xu, G.-F. Xu, D.-Z. Liao, K. Yoshimura, S.-P. Yan, P. Cheng, *Inorg. Chem.* **2007**, *46* , 8454.

Received: August 7, 2008
Published online: December 29, 2008

